Investigations of carbon nanotubes†

Ram Seshadri[1], A. Govindaraj[2], Hemantkumar N. Aiyer[3], Rahul Sen[3], G. N. Subbanna[3], A. R. Raju[3] and C. N. R. Rao[1, 2, 3]*

[1]Solid State and Structural Chemistry Unit, [2]CSIR Centre of Excellence in Chemistry and [3]Materials Research Centre, Indian Institute of Science, Bangalore 560 012, India

Experiments have been carried out to optimize the yields of carbon nanotubes obtained by the arc-evaporation of graphite. Other types of carbon particles such as nanocrystalline graphite usually present along with the nanotubes are readily removed by heating the material in oxygen around 763 K. Clean nanotubes so obtained have been characterized by X-ray diffraction. The clean tubes are thermally more stable than graphite or fullerenes. The tips of carbon nanotubes are opened by reaction with oxygen, but more interestingly, when the oxygen produced by the decomposition of a metal oxide is used to open the tube tips, the metal formed in the process enters the nanotube. Electrical resistance of pressed pellets of clean tubes is not unlike that of graphite. Tunnelling conductance measurements on isolated tubes characterized by means of scanning tunnelling microscopy however show that the conductance gap increases with decreasing tube diameter.

SINCE the discovery of carbon nanotubes in the cathodic deposit formed in the direct-current arc evaporation of graphite by Iijima[1], there has been considerable interest in the structure and properties of these nanomaterials. In this context, the report of Ebbesen and Ajayan[2] on methods to prepare nanotubes in larger quantities is of value. Smalley[3] has pointed out the importance of large electric fields in the plasma for the production of tubes. It has been possible to selectively burn tube tips and to strip the outer layers[4, 5]. The oxidative opening of the nanotube tips allows molten metal to be drawn in through capillary action[6]. Iijima and Ichihashi[7], and Bethune *et al.*[8] have reported catalysis by transition metals such as Fe and Co in the growth of single layer tubes. Besides carbon nanotubes, the other novel carbon structures that have attracted attention in recent months are the carbon onions first reported by Ugarte[9], consisting of closed concentric graphitic shells formed under conditions of strong heating. Theoretical calculations have indicated that carbon nanotubes may exhibit metallic or insulating behaviour, depending on their radius and helicity[10, 11]. Based on bias-dependent imaging studies in a scanning tunnelling microscope, Zhang and Lieber[12] suggest that nanotubes are semiconducting.

In view of the many interesting features of carbon nanotubes, we have investigated some aspects of their preparation and characterization, the main objective being the optimization of the preparative conditions, isolation of tubes without other contaminant carbon forms, and the characterization of clean tubes. Since the conditions for the arc production of nanotubes and fullerenes are quite complex, we have examined factors such as current and pressure in the production of these materials. We have also examined the effect of varying the gap between the electrodes in the plasma. Relative yields of nanotubes under different conditions have been studied based on scanning electron microscopy of the cathodic stub. We have then studied the oxidation of these materials including their thinning and opening. We show that most of the nanocrystalline graphite, usually present along with nanotubes, burns out on heating the material in oxygen. Such a cleaning process allowed us to determine the relative thermal stability of the nanotubes to graphite and the fullerenes. We have utilized powder X-ray diffraction data to assign the reflections and to draw some conclusions on the symmetries and correlation lengths.

In order to understand the electronic properties of carbon nanotubes, we have measured the resistivity as a function of temperature of pressed pellets of clean tubes as well as studied the tunnelling conductance of individual nanotubes of different diameters isolated by means of scanning tunnelling microscopy.

Experimental

Carbon nanotubes were generated by setting up an arc between 6 mm graphite electrodes (Johnson–Matthey, spectroscopic grade) in a water-cooled stainless steel chamber with one fixed and one moving electrode. The arc-gap was adjusted using a screw-feed mechanism with the distance between the electrodes being monitored visually through a viewport. The D.C. power supply used was a constant-current Indarc welding generator capable of providing up to 300 A with a maximum open circuit voltage of 60 V. Fullerene yields in the soot were monitored by extracting the soluble portion into toluene under ultrasonication and recording the electronic absorption spectrum of the toluene solution. Initial thermogravimetric analysis on a Cahn electrobalance in

*For correspondence

†Supported by the Jawaharlal Nehru Centre for Advanced Scientific Research, Bangalore 560 012, India

flowing oxygen showed that at 763 K, a small but perceptible weight loss occurs. The 'cleaning' of nanotubes was therefore performed by heating the mixture of tubes and carbon particles in flowing oxygen for 12 h at 763 K. The tendency to oxidation of clean nanotubes relative to graphite and fullerenes was studied by means of thermogravimetry. The simultaneous opening and filling of nanotubes with metal was done by heating clean nanotubes with Pb_3O_4 in flowing argon at 973 K for 9 h.

Scanning electron microscopy was carried out directly on the cathodic deposit (after coating it with gold) using a Cambridge Stereoscan S360 instrument operating at 20 kV. X-ray diffraction measurements were performed in the transmission geometry with the samples held between Mylar sheets on a STOE STADI with a linear position sensitive detector. $CuK_{\alpha 1}$ radiation was used. Silicon (NIST) was used as a reference for calibration purposes. Transmission electron microscopy was performed on a Jeol JEM 200 CX operating in the high resolution mode. The samples were ground in acetone and spotted on carbon-coated copper grids. Electrical resistance was measured on pressed pellets of cleaned nanotubes (10 tonnes over an area of 3.14 cm^2) using the four-probe configuration. Keithley meters and constant-current sources were used to study the resistance of samples mounted on the cold head of a helium closed cycle refrigerator.

Scanning tunnelling microscopy (STM) was performed with CCl_4 suspensions of nanotubes spotted on freshly cleaved highly oriented pyrolytic graphite (HOPG) substrates (a gift from Dr A. W. Moore, Union Carbide). A Nanoscope II, usually in the constant height mode was used for the purpose. Images were obtained with a typical bias of 600 mV. On obtaining stable images, the feedback loop was interrupted to obtain tunnelling spectra. Tunnelling spectra were obtained in air along the lengths of the tubes, after ensuring that the data referred to electron tunnelling, by monitoring the exponential dependence of tunnel current on tip-sample separation.

Results and discussion

Since the plasma characteristics are very important in the production of fullerene soot as well as of nanotubes, we first investigated the I–V behaviour of the plasma in 550 torr of helium. We show the results for two different gaps between the electrodes in Figure 1. For small electrode separations (say ~ 2 mm), the plasma is quite stable in the sense that the closed circuit voltage does not fluctuate, even at low currents. The plasma is steady and does not flicker, and the deposit on the cathode is cigar-shaped. The I–V behaviour is Ohmic with the resistance being of the order of 0.1 Ohm. This

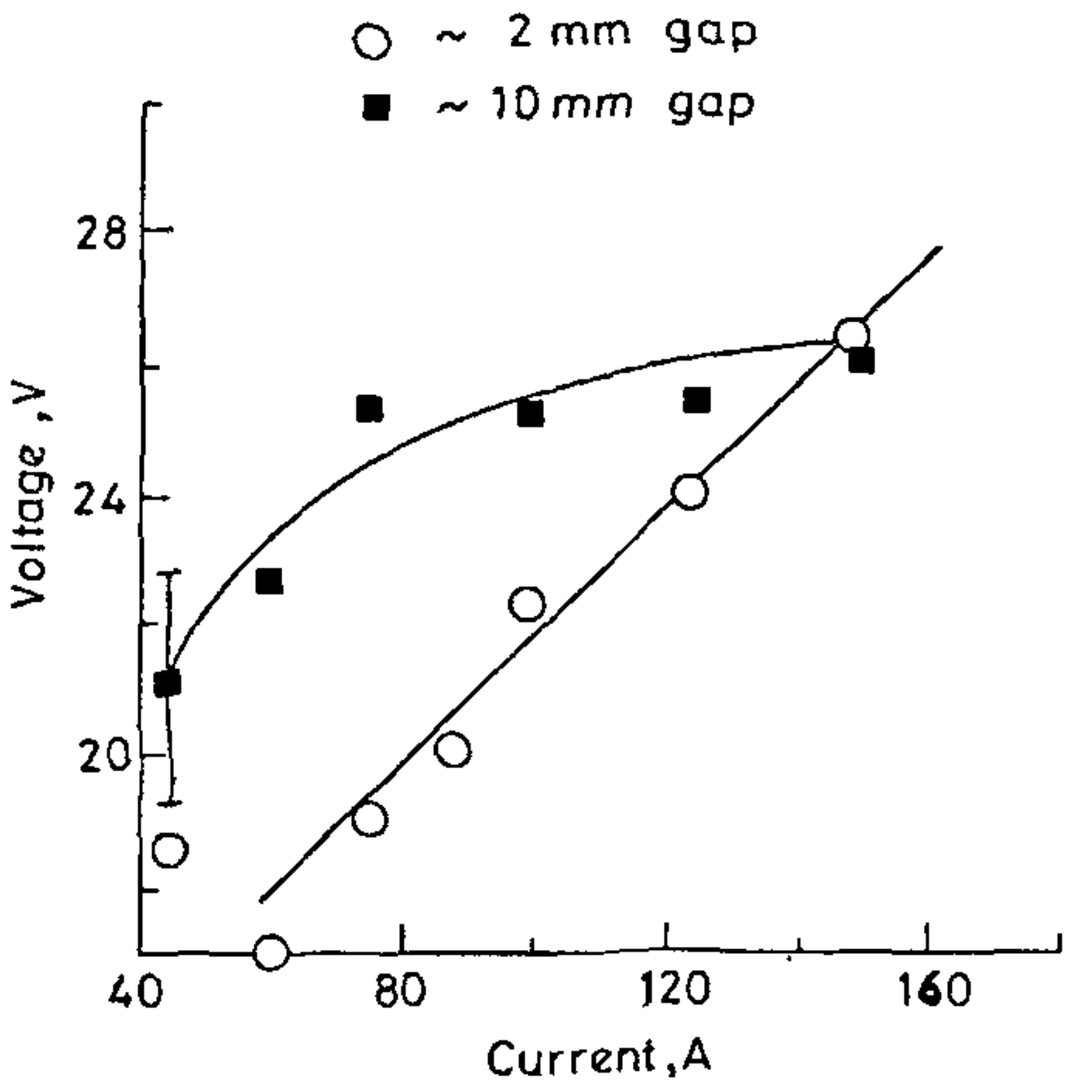

Figure 1. Current–voltage characteristics for the carbon plasma at 550 torr helium pressure at two different electrode separations, 2 mm and 10 mm. The separation was controlled visually and is only approximate The large error bar for the 10 mm separation at low currents reflects the instability of the plasma.

attests to the high density of the plasma and lends credence to the mechanism proposed by Smalley[3], which calls for a large dielectric constant in the plasma resulting in electric fields of the order of volts over distances of the order of bond lengths. When the electrode gap is increased to ~ 10 mm, the plasma is no longer stable at low currents and there is considerable fluctuation in the measured voltage. Visually, the plasma is seen to flicker. At constant current (up to ~ 120 A) the voltage is a fairly sensitive function of the separation between the electrodes, increasing with increasing separation as expected. The pressure of He in the chamber also modulates the voltage and hence the power dissipated at the electrodes. For a ~ 10 mm separation, for example, the voltage is 26 V in 50 torr of He and 33 V in 550 torr of He for a constant current of 150 A. It is our experience that low power favours the formation of nanotubes and hence, the pressure of He, the separation between the electrodes and the current used, all play a role.

We have monitored the variation in nanotube yields with different operating conditions by recording SEM of the cathodic stub formed on arc-evaporation of graphite. An SEM picture of a typical stub is shown in Figure 2*a*. The stub is about 5 mm across and has a soft black core covered by a hard grey slag. The slag is found to comprise mostly nanocrystalline graphite and very few tubes as can be seen in Figure 2*b*. This

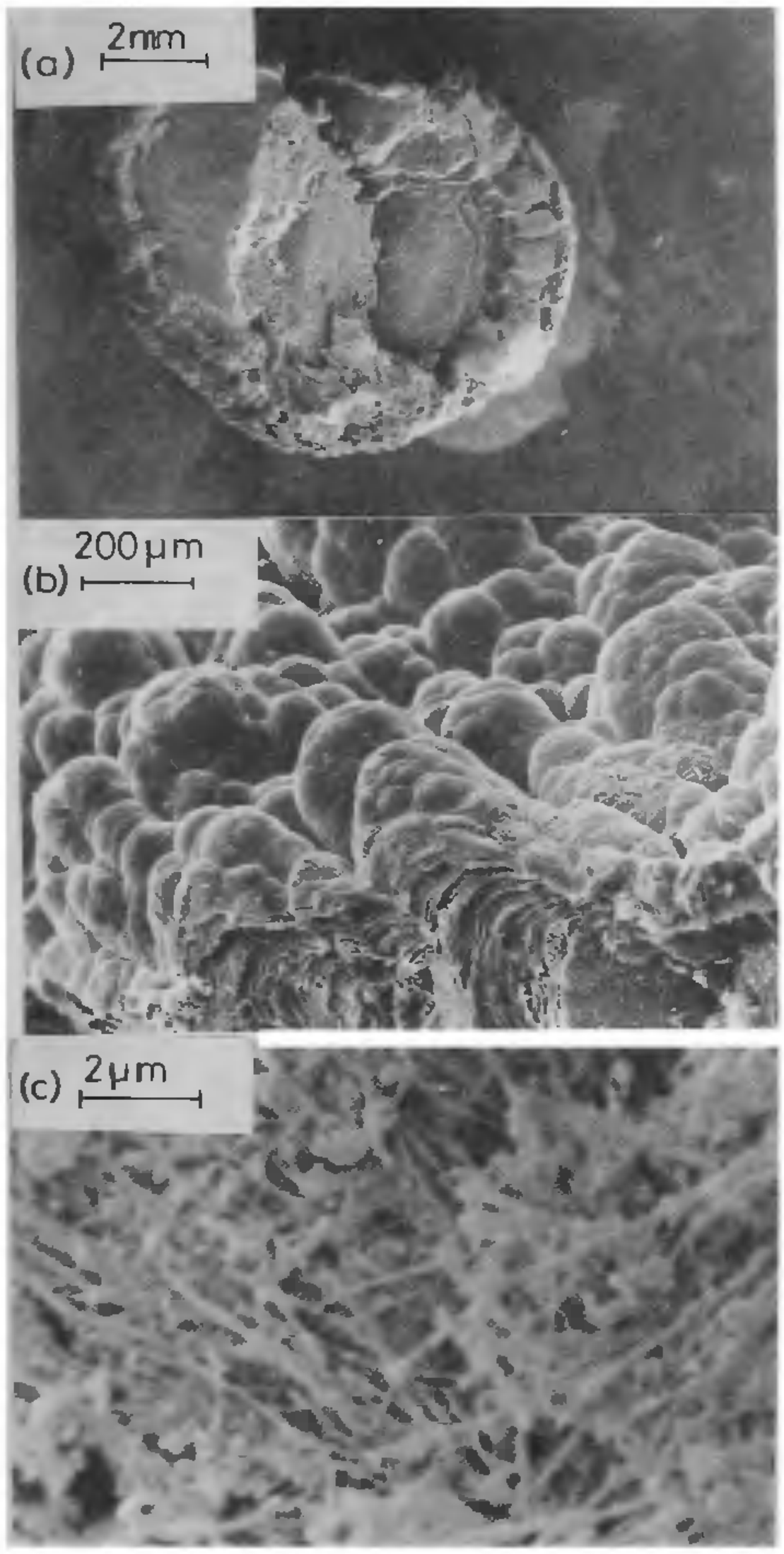

Figure 2. *a*, Low magnification SEM picture of a typical cathodic stub formed by arcing of graphite in 550 torr of helium. *b*, Magnified image of the slag on the stub. No tubes are seen even at higher magnification. *c*, Magnified image of the soft core portion of the stub showing the nanotube bundles. The separation between electrodes was 10 mm and the current, 60 A.

observation is consistent with the earlier literature reports[2,13] and is also supported by X-ray diffraction and TEM studies. At high currents of the order of 150 A and high pressures of 550 torr of He we find that vast quantities of soot are generated but the stub does not grow into the cigar-shaped object described earlier. Instead one mainly obtains a slag with very few tubes (as seen by SEM) composed essentially of nanocrystalline graphite. On decreasing the He pressure, and maintaining similar high currents, the tube yield remains low. Interestingly, the copious quantities of soot formed under these high current conditions have poor fullerene content. One of the interesting observations we have made is that at low pressure (50 torr) and high currents (up to 200 A), the anode, which is cylindrical and flat to start with, begins to sharpen in the plasma attesting to the extremely high fields. Under these conditions, tube yields are however, poor.

In the conditions of our experimental apparatus, i.e. making use of 6 mm diameter graphite rods, we are able to provide an optimal recipe for making carbon nanotubes. We find that at a He pressure of 550 torr and a current of 60 A, most of the material in the anode deposits on the cathode in the form of nanotube bundles. The production of soot is minimal at this pressure and current. Lower pressure or higher current result in the production of larger quantities of soot, whereas, current lower than 60 A result in unstable plasmas. The soft black core of the cathodic stub is surrounded by only a thin slag. Scanning electron micrographs of this central core (Figure 2*c*) show that it contains nanotubes in high yield. We verify this by examining SEM views along the stub axis as well cross-sections. The micrograph in Figure 2*c* is of a stub made with a 10 mm electrode separation. The tube bundles are distributed randomly. However with a 2 mm gap, the tube yields are high and the tubes are seen to be in aligned bundles. As mentioned earlier, tube formation is favoured when most of the anode is deposited on the cathode, and concomitantly, the soot yield is small. The production of nanotubes and of fullerenes are thus not complementary.

In order to determine whether we can improve tube yields, we have attempted a distillation by using the cathodic stub formed in one run as the anode in a new run. However, both SEM and HREM showed no observable difference in the yield of nanotubes before and after the distillation.

High resolution electron micrographs of the central core portion of the cathodic stub made in 550 torr of He and with 60 A current show tubes typically 1–2 µm long and 10–40 nm across. As observed by others, the tube tips are rarely perfectly conical[14]. Usually the tip is distorted and points to one side. The nanotubes are seen to be associated with small particles of nanocrystalline graphite. With as-prepared samples, it is difficult to distinguish these particles of nanocrystalline graphite from carbon onions, if they are present. Measurements of the lattice spacings in the HREM images as well as the separation of the 001 spots in the electron diffraction patterns give an interplanar separation of 3.4–3.45 Å.

Preliminary thermogravimetric analysis in oxygen of the core of the cathodic stub showed that at 763 K

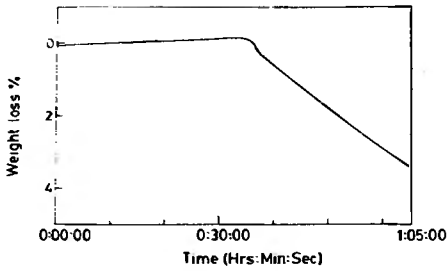

Figure 3. Isothermal TGA trace of a sample of carbon nanotubes and small graphite particles. After an initial ramp, the temperature was held at 763 K.

there is a small but perceptible weight loss (Figure 3). Assuming that the initial weight loss is due to the burning of small particles of nanocrystalline graphite rather than the nanotubes and other closed structures, we heated the mixture of nanotubes and nanocrystalline graphite in flowing oxygen at 763 ± 5 K for 12 h. Figure 4 shows the SEM of a sample so treated. We see that the surfaces of the tube bundles are cleaned by the treatment in the sense that very few graphitic particles remain. High resolution electron micrographs of nanotubes + onions from a sample obtained after 30% weight loss in air (post TGA) are shown in Figure 5. Onions and tubes are closed structures with no dangling bonds. This is why they are kinetically more inert toward combustion. Nanocrystalline graphite, which has a preponderance of dangling bonds, lacks this kinetic stability and burns away at lower temperatures. Figure 5 shows

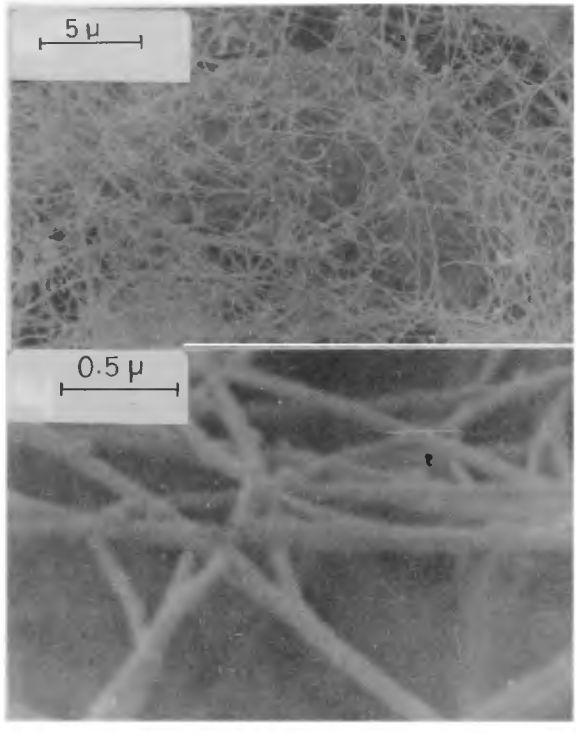

Figure 4. SEM pictures of a sample of nanotubes which have been heated in oxygen. The small graphitic particles are seen to have burnt away (cf. Figure 2 c).

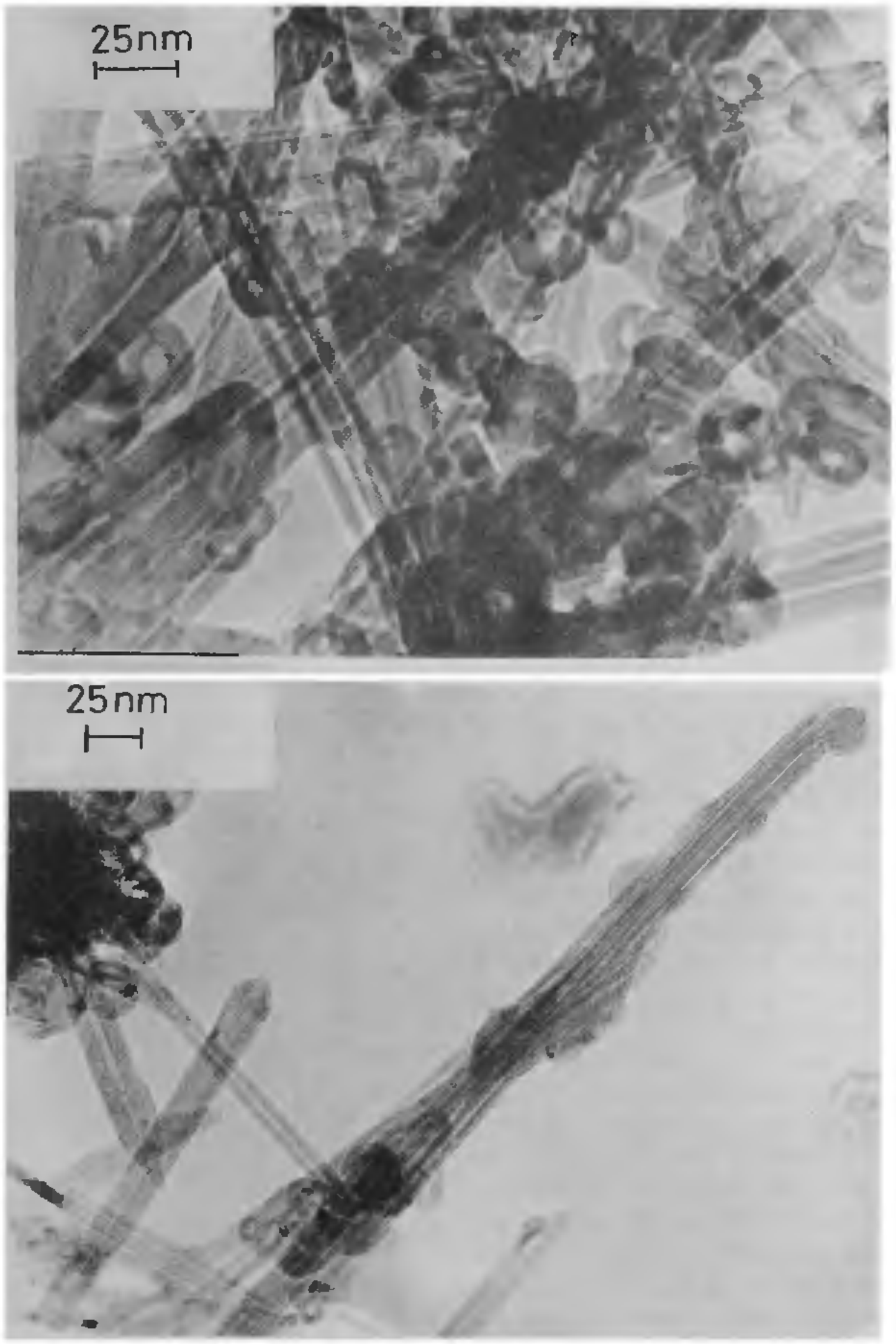

Figure 5. HREM of carbon nanotubes and onions obtained after 30% weight loss in thermogravimetry. Some of the nanotubes are thinned near the tips, where they are most susceptible to combustion. The onions are distinguished because graphitic nanoparticles have been burnt off.

that the nanotubes are thinner and sharper after the thermal treatment.

Nanotubes have five-membered rings at the tips necessary to close such cage structures. The five-membered rings render the tips more susceptible to oxidation because of the greater degree of strain associated with them. Thus air oxidation permits the opening of the tubes at the tips[4,5]. In Figure 6, we show a sample of nanotubes heated in air at 1023 K for 30 min. The tubes are seen to be open at the tips. The possibility of introducing an external material (e.g. a metal) inside a carbon nanotube has excited the imagination of many workers. A strategy to open and fill nanotubes is to heat them with a metal oxide which on decomposition gives oxygen and the free metal in the liquid state[5,6]. The liquid metal formed can get sucked into the tube soon after opening. We have tried such filling with lead metal by heating a sample of nanotubes with Pb_3O_4 in

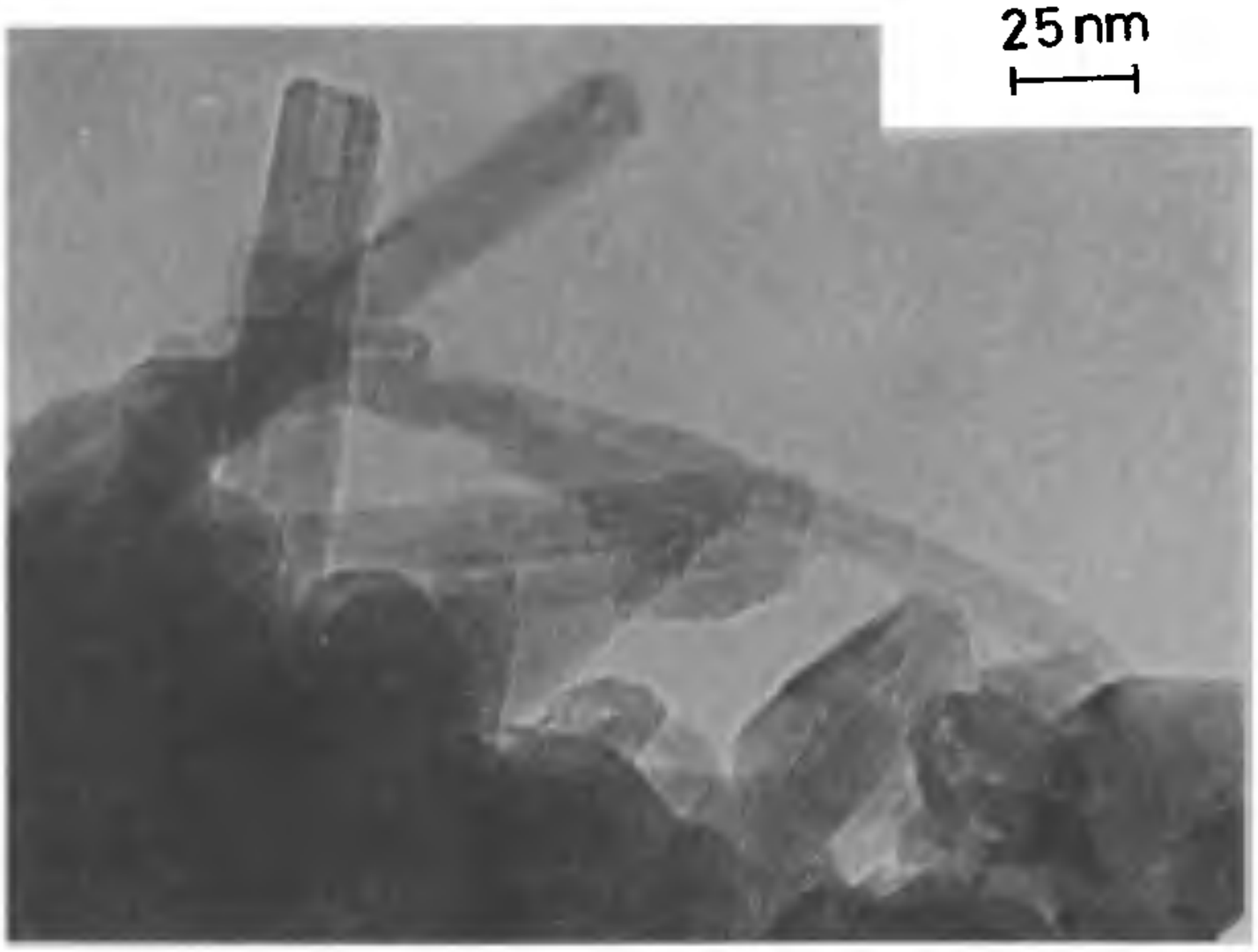

Figure 6. HREM of a sample of nanotubes with their tips opened by heating in air at 1023 K for 30 min

flowing argon at 973 K for 9 h and in Figure 7, we show an electron micrograph of a carbon nanotube so filled with lead. We were curious to know whether the lead was crystalline. The electron diffraction pattern of the filled metal, shown as an inset in Figure 7, corresponds to (111) spots of fcc lead indicating crystallinity of the metal. The lattice image of the (111) planes is also shown as an inset in Figure 7. Experiments are now underway to determine the properties of metals within such confined regions as nanotubes.

As a part of our efforts to characterize carbon nanotubes, we have recorded the powder XRD of the graphite starting material, the slag from the cathodic stub which we know from HREM to comprise mostly nanocrystalline graphite, and clean nanotubes. The XRD patterns (Figure 8) of graphite, slag as well as tubes show 00l reflections with squared Lorentzian lineshapes. However, both the tubes as well as the slag show no general *hkl* reflections and the *hk*0 reflections have a saw-tooth structure. Such patterns are well known for carbon blacks and other turbostratically modified graphites[15]. For tubes, the planes we expect Bragg reflections from are (00l) planes parallel to the tube axis, as well as planes perpendicular to the tube axis. For tubes with no helicity, or what have been referred to as armchair or serpentine tubes, the direction along the length of the tube is ⟨*h*00⟩ and we expect to see reflections from (*h*00) planes. For zigzag or sawtooth tubes, the direction along the length of the tube might be of the ⟨*hk*0⟩ e.g. ⟨110⟩ and we expect to see reflections from (*hk*0) planes. Since both 100 and 110 reflections

Figure 7. Micrograph of a nanotube encapsulating lead metal. Inset *a*, shows the selected area electron diffraction spots of the 111 planes of the encapsulated lead. Inset *b*, is a high resolution lattice image of the 111 plane.

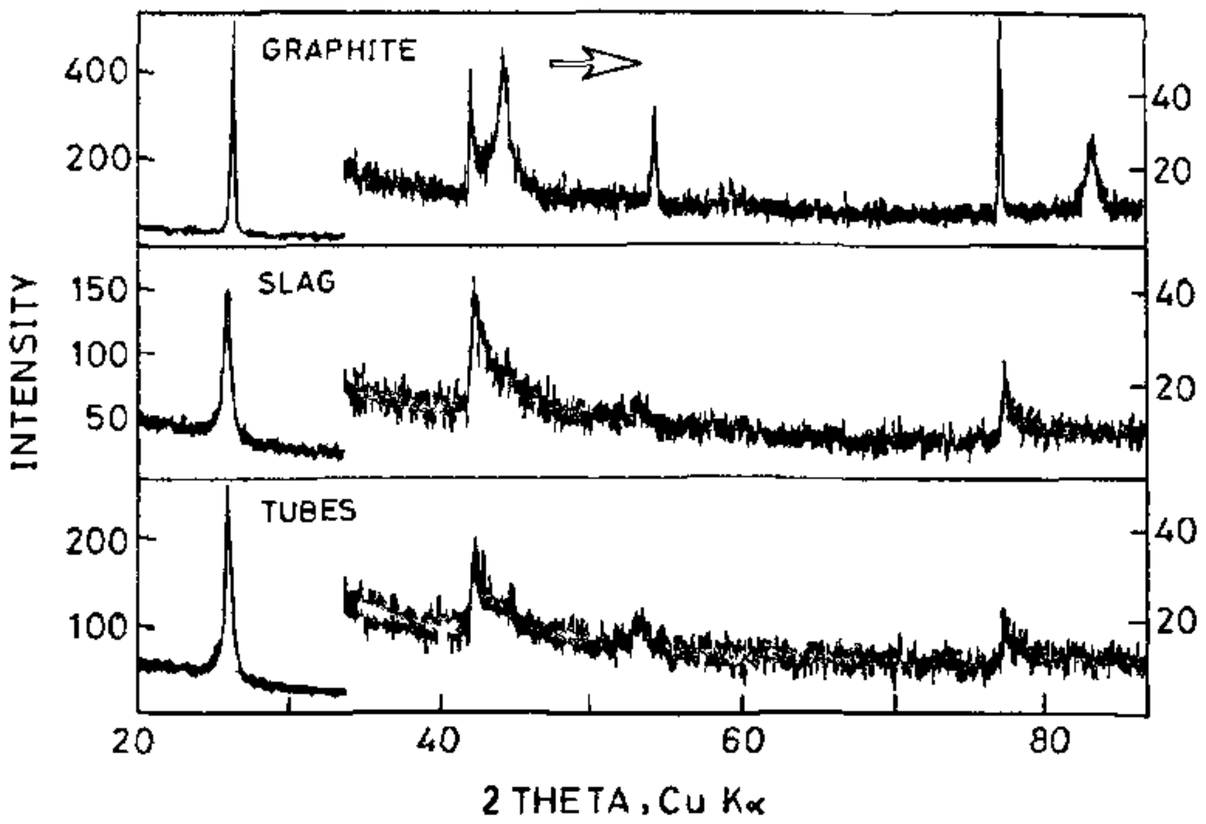

Figure 8. Powder X-ray diffraction patterns of graphite, the slag from the cathodic stub comprising mostly nanocrystalline graphite, and of clean nanotubes. Note the sawtooth *hk*0 reflections in the slag and the tubes, as well as the absence of general *hkl* reflections.

are of roughly equal intensity, we are tempted to say that we have a distribution of the two. However, the fact that the slag shows a very similar XRD pattern leads us to the more plausible explanation that these materials are quasi-2D in character, and that the patterns can be interpreted as arising from turbostratic modifications of graphite. The quasi-2D interpretation gains credence from the electrical transport data discussed presently. Also, calculations[16] on large fullerenes show that the graphitic portions between the points of curvature, i.e. the five-membered rings have a tendency to stay flat.

An early analysis of X-ray diffraction from random layer lattices, made by Warren[17], allows us to separately obtain correlation lengths for crystallinity in and perpendicular to the graphitic plane. In the plane, the correlation length L can be found from a knowledge of the peak shift $\delta\theta$, from the θ value for bulk graphite according to:

$$\sin(\delta\theta) = 0.16\,\lambda/L,$$

where λ is the wavelength of the X-ray used. One could also use peak broadening to obtain these correlation lengths. However, the measurement of broadening for unusual peakshapes is not a straightforward exercise. Our attempts to use peak broadening to determine correlation lengths result in values which are in very poor agreement with microscopy data. We have utilized

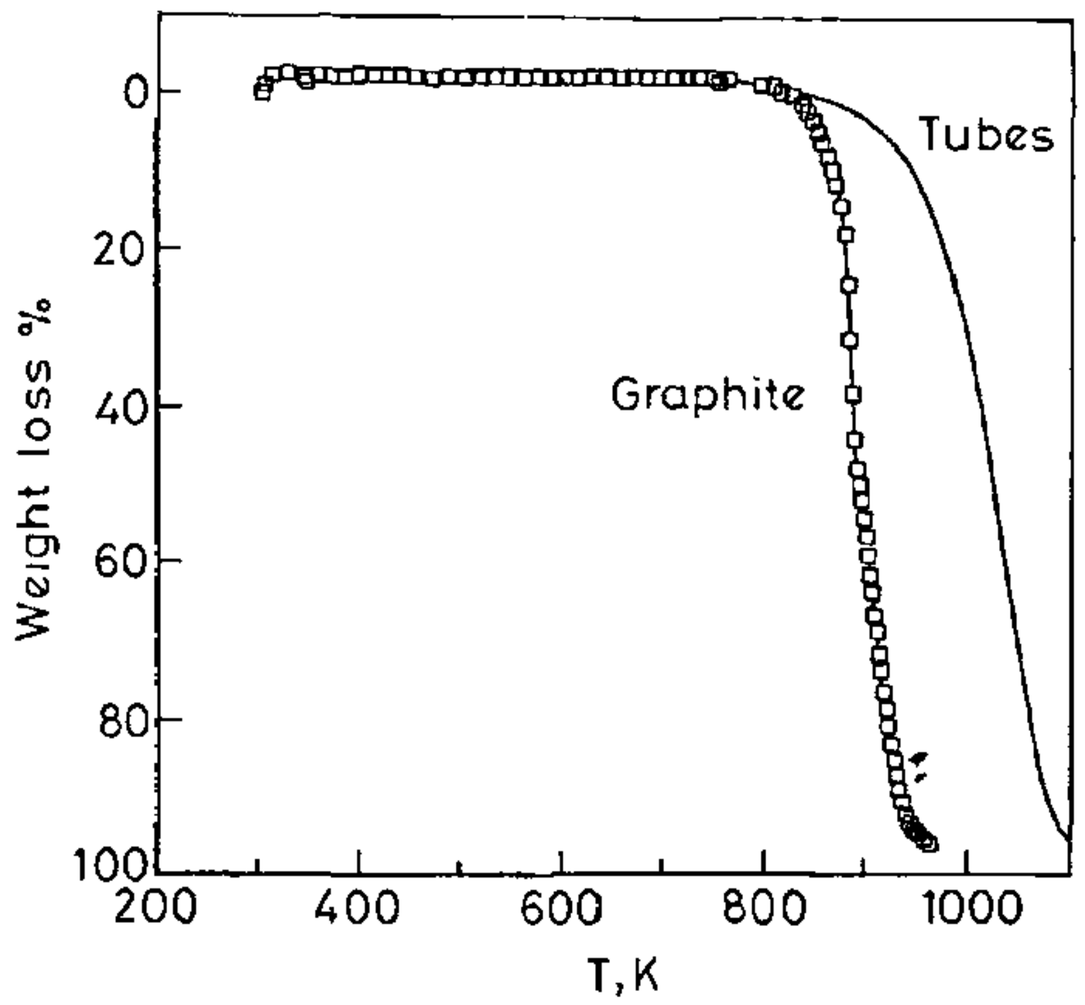

Figure 9. TGA traces (10 K/min, O_2 flow) of clean nanotubes and graphite powder. Note the relative inertness of nanotubes towards combustion.

Table 1. X-ray diffraction data of carbon nanotubes

Sample	2θ	*hkl*	Correlation length, nm *xy**	*z*†
Slag	26.075	002	–	15
	42.507	100	15	–
	77.495	110	22	–
Tube	26.021	002	–	17
	42.436	100	24	–
	53.311	004	–	12
	77.390	110	60	–
Graphite	26.487	002		
	42.312	100		
	44.438	101		
	54.416	004		
	77.320	110		
	83.413	112		

*Using the peak shift from bulk as suggested by Warren[17].
†Using standard peak-position vs. crystallite size plots, from Ruland[18].

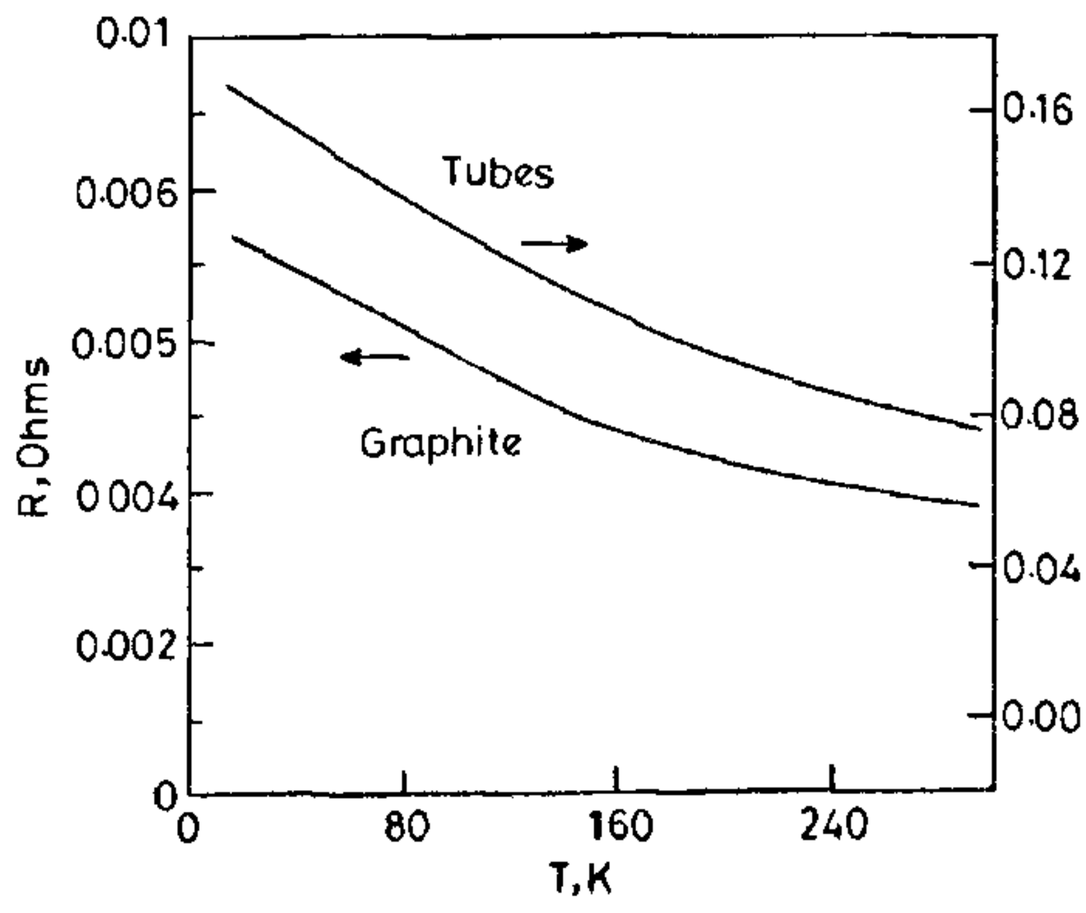

Figure 10. Temperature variation of the electrical resistance of a pressed pellet of clean nanotubes. Data for a pellet of graphite are also shown. The four probe geometry employed for the two samples was the same.

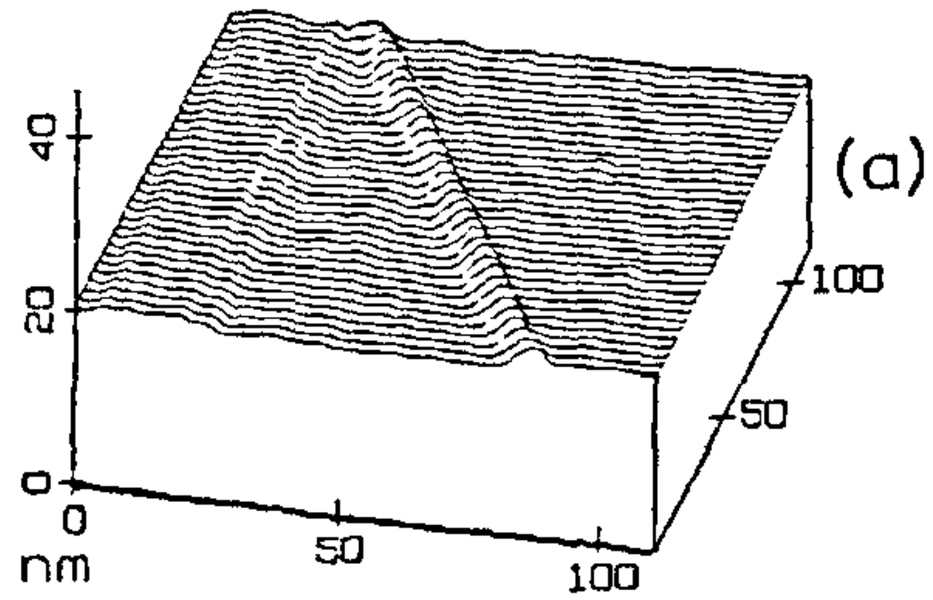

Figure 11. STM lineplots of nanotubes of different sizes on HOPG. The sizes are (*a*) 2.0 nm, (*b*) 3.0 nm and (*c*) 9.7 nm.

standard interplanar spacing-crystallite size curves[18] for graphite to obtain L along (001). The results of our X-ray studies are summarized in Table 1.

The availability of pure tube samples allows for reliable combustion studies to be made. In Figure 9, we compare the TGA trace of graphite with that of clean tubes (obtained by burning away the nanocrystalline graphite in flowing oxygen at 763 K for 12 h). The experiments were carried out in flowing oxygen at a

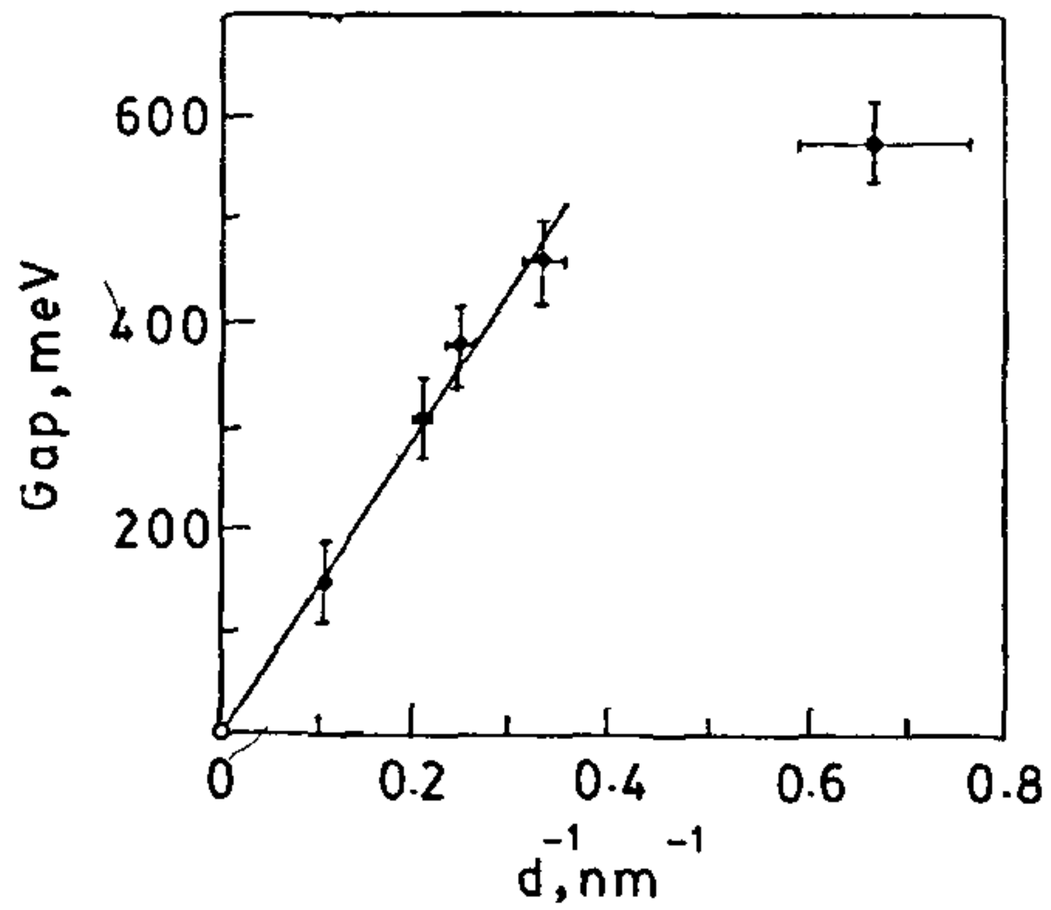

Figure 12. Plot of the conductance gap as a function of inverse diameter, d^{-1}. The origin corresponds to graphite which can be considered to be a tube of infinite diameter. The straight line is the best fit of the data (R_{fit} = 0.98) through the origin, and the points for the four larger tubes.

heating rate of 10 K/min. The first derivative of the data for clean tubes peaks at 1040 K, whereas the peak for graphite is at 920 K. Nanotubes clearly have an *extra kinetic stability over graphite. This is expected* since nanotubes have no dangling bonds and attack by oxygen radicals is more facile at the graphite sheet edge where carbon has unsaturated valences. Pang *et al.*[19] have recently reported a similar increased combustion temperature of nanotubes with respect to graphite. It should be noted that C_{60} burns away at a much lower temperature than either graphite or nanotubes because of the strain associated with the cage[19].

The four-probe resistance of a pressed pellet of clean tubes is shown in Figure 10 along with that of graphite. The resistance behaviour of the nanotubes is quite similar to that of graphite. The material is clearly a semiconductor with a very small band gap, which we estimate from ln(R) vs $1/T$ plots to be of the order of 1 meV. To obtain information on the electronic structure of individual tubes, we have carried out scanning tunnelling microscopy and spectroscopy studies. In Figure 11 we show STM lineplots of nanotubes of different diameters spotted on a HOPG substrate. In Figure 12 we have plotted the tunnelling conductance gap, measured from the flat portions of I–V curves against the inverse diameter, d^{-1} of the nanotube. The origin corresponds to the measurement on HOPG which could be considered an infinite diameter tube. The gap increases with decreasing diameter, linearly with d^{-1} for the larger tubes. This behaviour is known in other systems which show effects due to finite sizes[20]. From Figure 12, we observe that

the conductance gap of individual tubes is much larger than the activation gap obtained from the resistance data. This point is under further study. Tunnelling measurements in air, rather than in vacuum, can at best be partly responsible for some of the deviations.

1. Iijima, S., *Nature*, 1991, **356**, 56–58.
2. Ebbesen, T. W. and Ajayan, P. M., *Nature*, 1992, **358**, 220–223.
3. Smalley, R. E., *Mater. Sci. Engg.*, 1993, **B19**, 1–7.
4. Tsang, S. C., Harris, P. J. F. and Green, M. L. H., *Nature*, 1993, **362**, 520–522.
5. Ajayan, P. M., Ebbesen, T. W., Ichihashi, T., Iijima, S., Tanigaki, K. and Hiura, H., *Nature*, 1993, **362**, 522–524.
6. Ajayan, P. M and Iijima, S., *Nature*, 1993, **361**, 333–334
7. Iijima, S. and Ichihashi, T., *Nature*, 1993, **363**, 603–605
8. Bethune, D. S., Kiang, C. H., de Vries, M. S., Gorman, G., Savoy, R., Vazquez, J. and Beyers, R., *Nature*, 1993, **363**, 605–607.
9. Ugarte, D., *Nature*, 1992, **359**, 707–709.
10. Mintmire, J. W., Dunlap B. I., and White, C. T., *Phys. Rev. Lett.*, 1992, **68**, 631–634.
11. Hamada, N., Sawada, S and Oshiyama, A., *Phys. Rev. Lett.*, 1992, **68**, 1579–1581.
12. Zhang, Z and Lieber, C. M., *Appl Phys. Lett.*, 1993, **63**, 2792–2794.
13. Ebbesen, T W., Hiura, H., Fujita, J., Ochiai, Y., Matsui, S. and Tanigaki. K., *Chem. Phys. Lett.*, 1993, **209**, 83–90.
14 Ajayan, P. M., Ichihashi, T and Iijima, S., *Chem Phys. Lett.*, 1993, **202**, 384–388
15. Oberlin, A., in *Chemistry and Physics of Carbon* (ed. Thrower, P. A.), Marcel Dekker, New York, 1988, vol. 22, pp. 1–143.
16. Yoshida, M and Osawa, E., *Fullerene Sci. Technol.*, 1993, **1**, 55–74.
17. Warren, B E., *Phys. Rev.*, 1941, **59**, 693–698.
18 Ruland, W., in *Chemistry and Physics of Carbon* (ed. Walker, P. L.), Marcel Dekker, New York, 1968, vol. 4, pp. 1–84.
19. Pang, L. S. K., Saxby, J. D. and Chatfield, S. P., *J Phys. Chem.*, 1993, **97**, 6941–6942.
20 deHeer, W. A., Knight, W. D., Chou, M Y. and Cohen M. L., in *Solid State Physics* (eds. Ehrenreich, H. and Turnbull, D.), Academic Press, New York, 1987, vol. 40, pp 93–181.

Received 15 April 1994; revised accepted 17 May 1994

Analysis of the effects of amino acid sequence on the structure of proteins

S. Baranidharan and M. R. N. Murthy
Molecular Biophysics Unit, Indian Institute of Science, Bangalore 560 012, India

The conformation of amino acid side chains as observed in well-determined structures of globular proteins has earlier been extensively investigated. In contrast, the structural features of the polypeptide backbone that result from the occurrence of specific amino acids along the polypeptide have not been analysed. In this article, we present the statistically significant features in the backbone geometry that appear to be a consequence of the occurrence of rotamers of different amino acid side chains by analysing 102 well-refined structures that form a random collection of proteins. It is found that the persistence of helical segments around each residue is influenced by the residue type. Several residues exert asymmetrical influence between the carboxyl and amino terminal polypeptide segments. The degree to which secondary structures depart from an average geometry also appears to depend on residue type. These departures are correlated to the corresponding Chou and Fasman parameters of amino acid residues. The frequency distribution of the side chain rotamers is influenced by polypeptide secondary structure. In turn, the rotamer conformation of side chain affects the extension of the secondary structure of the backbone. The strongest correlation is found between the occurrence of g^+ conformation and helix propagation on the carboxyl side of many residues.

THE central dogma of protein folding holds that the three-dimensional structure of proteins is completely determined by their respective amino acid sequence. This implies that the occurrence of each amino acid along the polypeptide chain influences the polypeptide fold individually as well as in association with residues that occur in close proximity. In light of this, it is surprising that no detailed analyses of the stereochemical effects resulting from the occurrence of specific amino acids along the polypeptide chain are available in the literature. In contrast, the conformations of individual amino acids as observed in proteins have extensively been studied[1–6]. Janin *et al.*[3] analysed the high resolution protein structures available at that time and reported frequency distribution of different side chain conformations of all amino acids. It was observed that χ_1 ($N - C_\alpha - C_\beta - C_\gamma$ angle) distribution is trimodal with g^- conformation (C_γ trans to H_α) rare and g^+ (C_γ trans to C') position preferred in most amino acids. They also reported the estimates of deviations of the dihedral angles from the g^-, t (C_γ trans to N) and g^+ positions. Ponder and Richards[5] reexamined side chain conformations and observed that 67 distinct side chain rotamers account for most of the conformations of 17 of the 20 amino acids. Similar restricted set of conformational